ACS OMEGA

Open Access

http://pubs.acs.org/journal/acsodf

Article

Physiologically Based Pharmacokinetic Model of Plasma and Intracranial Pharmacokinetics and CDK4/6 Occupancy of Abemaciclib to Optimizing Dosing Regimen for Brain Metastatic Patients

Chao Zhang, Shan Li, Jiawei Ren, and Ren Lang*

Cite This: *ACS Omega* 2025, 10, 9245−9256

Read Online

ACCESS | Metrics & More | Article Recommendations | Supporting Information

ABSTRACT: *Objective*: The study aimed to develop a physiologically based pharmacokinetic (PBPK) model to predict steady state trough concentrations (C_{min}) and CDK4/6 occupancy in plasma and cerebrospinal fluid (CSF) for abemaciclib (ABE) and its three active metabolites. Additionally, a biomarker model was constructed to simulate changes in pRB and TOPO-IIα expression. *Methods*: The population PBPK and biomarker models of ABE were developed using physicochemical, pharmacokinetics (PK), CDK4/6 occupancy, biomarker, and physiological properties. These models were then validated using four clinical plasma PK studies, two CSF PK studies, and one clinically observed biomarker expression change in patients. *Results*: The PBPK model showed good consistency with observed data, with most prediction-to-observation ratios falling within the range of 0.5 to 2.0 for AUC, C_{max}, C_{min} in plasma and CSF. Key factors affecting C_{min} and CDK4/6 occupancy for total analytes (sum of ABE and metabolites) were identified as CYP3A4, ABCB1, ABCG2 expression, and plasma albumin levels. PBPK simulations suggested that the optimal dosing regimen for ABE in brain metastatic breast cancer (MBC) is either 150 or 200 mg twice daily (BID). *Conclusions*: The PBPK model successfully simulated the PK profiles and CDK4/6 occupancy for ABE and its three metabolites in plasma and CSD, and determined the optimal dosing in brain MBC. Overall,The PBPK model can provide important insights for personalized dosing strategies, contributing to improved treatment efficacy and safety for patients, particularly those with brain MBC.

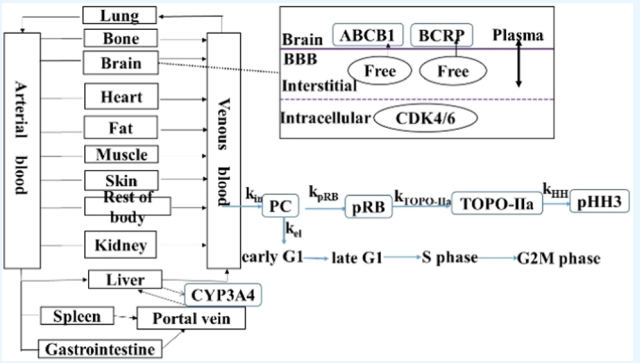

1. INTRODUCTION

Breast cancer (BC) stands as the most prevalent cancer among women and ranks as the second leading cause of cancer-related mortality in this demographic.[1] Metastatic breast cancer (MBC) was estimated to affect over 150,000 women.[2] MBC includes various histopathological subtypes distinguished by the expression of receptors, such as the estrogen receptor (ER), progesterone receptor (PR), and human epidermal growth factor receptor 2 (HER2). Among these, hormone receptor (HR) positive, HER2 negative BC emerges as the most common subtype.[3] Despite advancements in early-stage disease management, approximately one-third of the patients inevitably progress to metastatic stages. MBC remains incurable, and the 5-year survival rate fluctuates around 25%.[4] Additionally, BC is the second leading cause of brain metastases development after lung cancer.[5] Among all MBCs, the incidence of brain metastases is relatively high, with reported rates of 31, 32, and 15% in patients with HER2-positive, triple-negative, and HR-positive/HER2-negatve BC, respectively.[6] Patients with brain MBC exhibit a shorter survival rate compared to those without, at 26.3 versus 44.6 months,[6] and face limited treatment options. Ensuring effective drug delivery into the brain remains a crucial challenge.[5,6] The extent of blood-brain barrier function and its characteristics can vary among brain MBC. For instance, brain metastases from HER2-positive BC typically express higher levels of GLUT1 and ABCG2 compared to other subtypes, which can further limit free drug concentration in brain.[7]

Cyclin-dependent kinase (CDK) 4 and 6 are activated upon binding with D-cyclins, playing a pivotal role in signaling pathways that drive cell cycle progression and cellular proliferation.[8] These kinases have been demonstrated to facilitate protein (RB), thereby promoting cellular proliferation

Received: October 18, 2024
Revised: February 11, 2025
Accepted: February 19, 2025
Published: February 24, 2025

Table 1. Input Parameters for Abemaciclib and Active Metabolites in PBPK Model for Patients[a]

	parameters (units)	ABE	M2	M18	M20	source and comments
physicochemical	M_W (g·mol^{-1})	506.6	478.5	494.5	522.6	ref31
	pK_a (base)	4.48, 7.95	9.19	9.19	8.37	
	log P	3.36	3.66	2.35	2.78	
	GET (min)	190				
	f_{up}	0.039	0.093	0.046	0.030	calculated using eq 2, original data was from ref14
absorption	P_{eff} ($\times 10^{-4}$ cm·s^{-1})	2.46				ref31
	Weibull time (min)	90				optimized based on peak time of PK profiles
	Weibull shape	0.92				
distribution	R_{bp}	0.98	0.98	0.80	0.81	calculated using eq 3, original data was from ref14
	$K_{CSF,P}$	0.68	0.14	1.0	0.91	calculated based on the data from ref16,33
	K_p scale	5.0				optimized based on PK profiles
elimination	CYP3A4 $CL_{int,u}$ (μL/min/pmol)	0.634[a], 0.117[b], 0.576[c]	0.487[d]	0.197	0.444	a,b: CYP3A4-mediated clearance pathway of ABE that forms M2 and M18, respectively; c: clearance pathway of ABE that forms other metabolites; d: CYP3A4-mediated clearance pathway of M2 that forms M20. ref31
	HLM $CL_{int,u}$ (μL/min/mg)	9.733	50.0	160	21.37	ref31
	CL_R (L/h)	1.0				
	ABCB1 $CL_{int,u}$ (pmol/min)	0.27	2.27		1.30	calculated based on transported ABE, M2 and M20 amount in 4 h, ref15
	ABCG2 $CL_{int,u}$ (pmol/min)	0.095	1.19		0.60	
concentration	CYP3A4	3.02				ref30
	ABCB1	1.3				abundance values were obtained from ref 34 and then calculated: abundance multiplied by milligrams of protein per gram of tissue multiplied by brain weight
	ABCG2	2.4				
CDK4/6 occupancy	K_d (nM) for CDK4/6	0.6/8.2	1.2/1.3	1.2/2.7	1.5/1.9	ref15 for three metabolites and ref35 for ABE
	k_{off} (min^{-1})	0.10				fitted through nonlinear analysis using the data from ref 36 for ABE, three metabolites were assumed to be identical
biomarker	k_{RB} (h^{-1})	0.16				k_{To} and k_{To} were optimized based on the clinical study data, ref16; The remaining rate constants were taken from the ref37
	k_{TO} (h^{-1})	0.14				
	k_{HH} (h^{-1})	0.21				
	k_{el}	0.05				
physiological	hematocrit	0.33				mean value in patients from ref30
	albumin (g/dl)	3.1				

[a] M_W: molecular weight; pK_a (base): base dissociation constant; log P: lipophilicity; GET: gastric emptying time; f_{up}: free fraction in plasma; P_{eff}: human effective permeability; Weibull time and shape: dissolution time of 50% ABE and shape parameter of Weibull function; R_{bp}: blood-to-plasma concentration ratio; $K_{CSF,P}$: cerebrospinal fluid-to-plasma partition coefficient; K_p scale: organ-to-plasma partition coefficient; CYP3A4 $CL_{int,u}$ and HLM $CL_{int,u}$: intrinsic clearance for CYP3A4 and human liver microsomes; CL_R: renal clearance; ABCB1 $CL_{int,u}$ and ABCG2 $CL_{int,u}$: intrinsic transport velocity for ABCB1 and ABCG2; K_d: equilibrium constant between drug-CDK binding; k_{off}: first-order dissociation rate constant from CDK4/6; k_{RB}: rate constant from early G1 to late G1 phase; k_{To}: rate constant from late G1 to S phase; k_{HH}: rate constant from S to G2M phase; k_{el}: elimination constant from the precursor compartment.

and tumor growth. CDK4/6 were identified as therapeutic targets in cancer treatment in the late 1990s and early 2000s, and CDK4/6 inhibitors have been demonstrated as effective drugs for BC patients.[9,10]

Abemaciclib (ABE) stands as an oral selective small molecule inhibitor targeting CDK4/6, effectively hindering the phosphorylation of the retinoblastoma (pRB) and the expression of topoisomerase-IIα (TOPO-IIα).[11,12] This inhibition prevents the progression from the G1 to the S phase in the cell cycle, thereby arresting tumor growth.[12] ABE primarily undergoes metabolism by the enzyme CYP3A4.[13] Notably, in human plasma, the major active metabolites identified are M2, M18, and M20, contributing 13, 5, and 26% of the total plasma mass *in vivo*,[14] respectively. Importantly, their inhibition toward CDK4/6 mirrors that of ABE.[14] Furthermore, *in vitro* studies have revealed that ABE acts as a substrate for the efflux transporters ABCB1 (P-glycoprotein) and ABCG2 (breast cancer resistance protein).[15] ABE has demonstrated a notable ability to penetrate the cerebrospinal fluid (CSF), with free concentrations reaching approximately 68% of those observed in plasma.[16] This significant penetration into the brain holds promise for achieving therapeutic concentrations, presenting a promising approach for treating brain MBC. To date, the clinical study has shown the efficacy of ABE in treating patients with brain MBC.[17]

There is a notable degree of variability in the pharmacokinetics (PK) of ABE, with a percentage coefficient of variation (%CV) exceeding 70% and, in some instances, even surpassing 100%.[16] This variability in the PK can be influenced by genetic polymorphisms of the CYP3A4 enzyme, which plays a pivotal role in ABE metabolism. Wild-type carriers of CYP3A4 exhibit higher expression and activity by 1.7- and 2.5-fold, respectively, compared to carriers of the CYP3A4*22 allele (*1/*22 and *22/*22).[18] Furthermore, variations in polymorphisms of

https://doi.org/10.1021/acsomega.4c09472
ACS Omega 2025, 10, 9245−9256

efflux transporters among patient groups can also contribute to PK variability. A functional variant of ABCB1 and ABCG2 has been associated with greater drug accumulation.[19] Efflux ratios can increase significantly by approximately 4-fold due to polymorphisms of ABCB1 or ABCG2.[19,20] Additionally, several studies have highlighted the significant impact of albumin levels on clinical efficacy of a drug in patients.[21,22] Additionally, some studies have revealed substantial variations in albumin levels among cancer patients, ranging from 0.28 to 5.8 g/dL.[23,24] ABE demonstrates a high plasma protein binding rate of close to 96%.[14] Moreover, the research has demonstrated a statistically significant correlation between albumin levels and the adverse events of ABE in BC patients.[25]

For certain kinase inhibitors, maintaining a sufficient plasma trough concentration at steady state (C_{min}) is often critical for achieving clinical efficacy.[26] While a C_{min} of 200 ng/mL was established as an effective concentration threshold using a mouse xenograft model,[13] this finding lacks direct clinical relevance as it did not consider the on-target effects of active metabolites of ABE. Several studies have demonstrated a strong correlation between the level of BTK engagement and clinical response rates.[27,28] Zanubrutinib achieved nearly 100% engagement of BTK at steady state, which significantly contributed to better clinical responses.[27] Another study indicated that acalabrutinib achieved over 90% occupancy of BTK, resulting in a response rate exceeding 80%.[28] Based on these findings, it has been suggested that achieving at least 90% engagement by ABE in CSF could serve as an effective threshold for clinical efficacy. The exposure−response relationship for safety demonstrated a strong positive correlation between C_{min} of total active analytes (sum of ABE, M2, and M20) and neutrophil counts.[14] Due to the observed grade 3 fatigue in a significant proportion of patients at the 275 mg twice daily (BID) dose, the C_{min} of total active analytes at 275 mg BID was determined as the maximal concentration threshold for clinical safety.[14]

Physiologically based pharmacokinetic (PBPK) models have extensive application in simulating drug concentrations in human plasma and CSF,[29,30] as well as predicting target occupancy.[22,28] Two PBPK studies for ABE have been reported.[31,32] In Posada's study,[31] they investigated the dosing considerations of ABE when it was administered concurrently with CYP3A4 perpetrators in healthy volunteers. However, their approach was primarily based on the conventional method of determining the ABE dosage through plasma AUC ratios. Additionally, in Li's study,[32] they developed a PBPK model of ABE to predict ABE concentrations in CSF and guide dosing selection for patients. However, this approach did not take into account the differences in modeling parameters between healthy and diseased populations as well as the effects of the three active metabolites on clinical efficacy. Our research differs from theirs in three ways: (i) We refined several parameters within our PBPK model, including CYP3A4 expression, albumin levels, GET, hematocrit, f_{up}, and R_{bp}, to better simulate C_{min} of ABE in patients, which differ between healthy and diseased populations. Notably, our PBPK model is capable of predicting the C_{min} of ABE and its three active metabolites simultaneously in human plasma and CSF. (ii) In contrast to Li et al.'s methodology, which primarily uses the ratios of C_{min} and IC_{50} as a rough predictor of efficacy when guiding ABE dosing selection, we determined the optimal ABE dosing regimen by assessing both efficacy, through CDK4/6 occupancy in CSF, and safety, via plasma C_{min} of total ABE analytes. (iii) Our PBPK model also analyzed additional factors influencing C_{min} and CDK4/6 occupancy by ABE in plasma and CSF, as well as simulated the changes in two biomarkers (pRB and TOPO-IIa) over time following ABE administration. This work can provide important insights into personalized dosing strategies of ABE for patients with brain MBC.

2. METHODS

2.1. PBPK Model Development. A comprehensive whole-body PBPK model was constructed to predict plasma and intracranial PK and CDK4/6 occupancy for ABE and its three active metabolites. The model was developed by using PK-Sim software (Version 9.1, Bayer Technology Services, Leverkusen, Germany). System-specific parameters were predominantly sourced from the existing PK-Sim database unless explicitly specified otherwise. Detailed drug-specific parameters, CDK4/6 occupancy, biomarker-related, and physiological-related parameters for patients are presented in Table 1.[14−16,30−37]

To simulate ABE absorption in the gastrointestinal tract, we employed the Weibull absorption model, which is characterized by its time and shape parameters. The Weibull time parameter was optimized to 90 min to align better with the peak time of PK profiles. The distribution of ABE to various organs/tissues and cellular permeability calculations were determined using the built-in Rodgers and Rowland method and the standard PK-Sim. Furthermore, the organ-to-plasma partition coefficient (K_p scale) was optimized to 5.0 for improved description of ABE distribution module in PK-Sim. This optimization was achieved through the parameter identification module, while all other parameters were fixed. The model also accounted for the active efflux clearance of ABE mediated by ABCB1 and ABCG2. The intrinsic transport velocities ($CL_{int,u}$ values) of ABCB1 and ABCG2 for ABE, M2, and M20 were calculated based on the ratio of transported amounts of ABE, M2, and M20 over a 4 h period.[15]

In the PK-Sim model, the brain tissue was compartmentalized into four segments: plasma, blood cells, interstitial space, and intracellular space.[30] For this simulation, in order to predict the free concentration of ABE and the three metabolites in the CSF, the unbound concentration in the interstitial fluid was presumed to be equivalent to the free concentration in the CSF, based on a previous study.[30] The CSF-to-plasma concentration ratio ($K_{CSF,p}$) for ABE was set at 0.68, based on the mean ratio of ABE free concentration between the CSF and plasma.[16] Additionally, according to data from the referenced paper,[33] $K_{CSF,p}$ values were determined to be 0.14 for M2 and 0.91 for M20. However, as no data were available for M18, $K_{CSF,p}$ was assumed to be 1.0 for this metabolite.

The CDK4/6 occupancy is calculated based on the published paper by[38]

$$\frac{dN}{dt} = \frac{k_{off}}{K_d} \times CDK_{unbound} \times C_{drug} - k_{off} \times CDK_{bound} \quad (1)$$

where dN/dt represents the change of drug-CDK complex formed over time. k_{off} is the first-order dissociation rate constant. K_d is the equilibrium constant for drug-CDK binding. $CDK_{unbound}$ is the concentration of unbound CDK4/6. CDK_{bound} is the amount of the drug-CDK4/6 complex. C_{drug} represents the free drug concentration in plasma or the CSF.

https://doi.org/10.1021/acsomega.4c09472
ACS Omega 2025, 10, 9245−9256

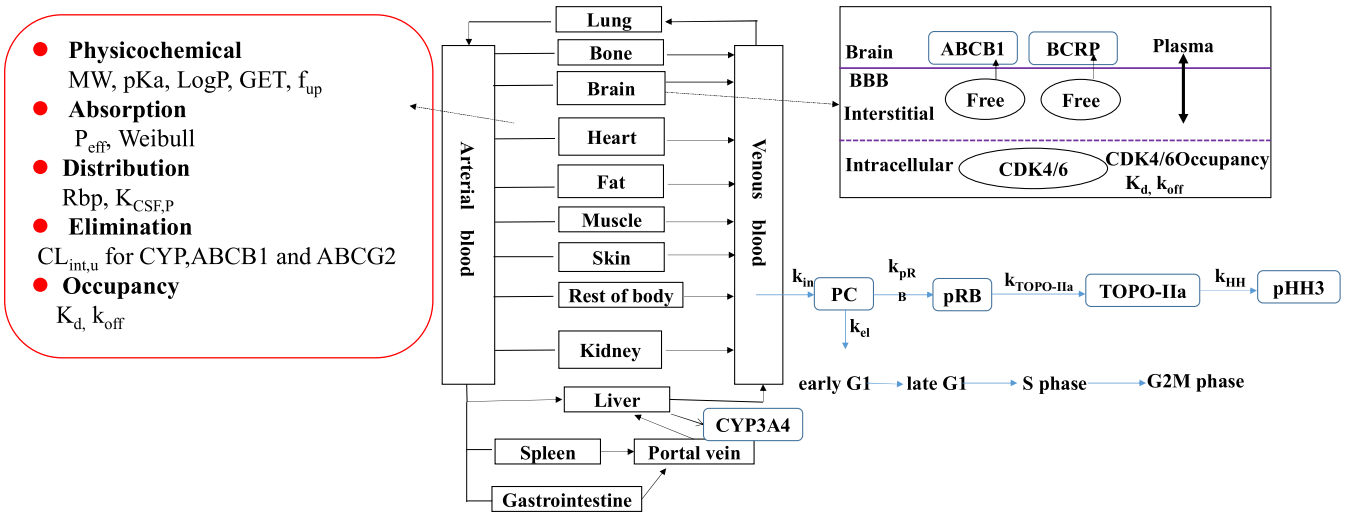

Figure 1. Schematic diagram of the PBPK and biomarker model for ABE. The PBPK model is composed of the gastrointestinal tract, the circulatory system (including both arterial supply and venous return), the eliminating tissues (such as the liver and kidneys), and other noneliminating tissues (such as lung and bone). These compartments are connected through a blood flow. ABE undergoes metabolism in the gastrointestinal tract and liver by CYP3A4, and effluxes by ABCB1 and ABCG2 on BBB. Within the model, the brain is a specialized compartment that includes not only the brain tissue but also the subcompartments referred to as plasma, blood cells, and interstitial and intracellular spaces. The biomarker model is composed of four transit compartments, where PC represents cell accumulation in early G1 in precursor compartment; k_{in} and k_{el} represent rate constant into the precursor compartment and elimination rate constant from the precursor compartment, respectively. k_{pRB}, $k_{TOPO\text{-}II\alpha}$, k_{HH} represent the rate constants from early G1 to late G1, from late G1 to S phase, and from S phase to G2M phase, respectively.

CDK4/6 occupancy was calculated as the percentage of the CDK4/6 that was binding to the ABE and metabolites at a particular time point. After the dosing of the ABE, CDK4/6 occupancy of ABE and the three active metabolites were simulated in the same manner simultaneously, and the sum of the occupancy by ABE and metabolites gave the total CDK4/6 occupancy. The starting expression of CDK4/6 ($CDK4/6_0$) was set at default 0.1 μM due to not reported data in human.

In the PBPK model, various modeling parameters for BC populations differed from those for healthy populations, as documented in previous publications.[30] The expression level of CYP3A4 was reduced to 3.02 μM compared to the healthy population's 4.32 μM.[30] Additionally, compared to healthy subjects, albumin levels (g/dL) and hematocrit in patients were also reduced from 4.5 to 3.1 and from 0.43 to 0.33,[30] respectively. The parameters f_{up} and R_{bp} in BC patients were scaled using eqs 2 and 3[30]

$$f_{up} = 1/(1 + ((1 - f_{up}) \times [\text{Albumin}_p]) /([\text{Albumin}_h] \times f_{up,h})) \quad (2)$$

where f_{up} and $f_{up,h}$ is the free plasma fraction, and $[\text{Albumin}_p]$ and $[\text{Albumin}_h]$ are the plasma albumin levels in patients and healthy subjects, respectively.

$$R_{bp} = 1 + \text{Hct} \times (f_{up} \times (\text{Hct} - 1 + R_{bp,h})/(\text{Hct} \times f_{up,h}) - 1) \quad (3)$$

where R_{bp} and $R_{bp,h}$ are the blood-to-plasma concentration ratio in patients and healthy subjects, respectively; Hct is the hematocrit value.

2.2. Biomarker Model Development. The RB is an important regulatory factor controlling the cell cycle, capable of preventing cells from entering the S phase from the G1 phase. Additionally, in many types of cancers, including BC, the expression level and activity of TOPO-IIα may be increased, because it also plays a crucial role in the rapid proliferation and division of tumor cells. Therefore, in BC, the inactivation of RB protein and the overexpression of TOPO-IIα may serve as markers for disease progression and treatment response.[14,35] The biomarker model was constructed to simulate the temporal changes of two biomarkers, pRB and TOPO-IIα, in BC patients, following ABE administration. This model consisted of four transit compartments, as detailed in the referenced paper, encompassing early G1, late G1, S phase, and G2M cell cycle phases in a sequential manner.[37] The biomarker model is delineated as follows:

$$\frac{dPC}{dt} = k_{in} - k_{el} \times PC - k_{pRB} \times PC \times (1 - CO) \quad (4)$$

$$\frac{dpRB}{dt} = k_{pRB} \times PC \times (1 - CO) - k_{TOPO\text{-}IIa} \times pRB \quad (5)$$

$$\frac{dTOPO\text{-}II\alpha}{dt} = k_{TOPO\text{-}IIa} \times pRB - k_{HH} \times TOPO\text{-}II\alpha \quad (6)$$

where PC represents the cell accumulation in early G1 in the precursor compartment; k_{in} and k_{el} represent the rate constant into the precursor compartment and elimination rate constant from the precursor compartment, respectively. CO is the CDK occupancy fraction. k_{pRB}, $k_{TOPO\text{-}II\alpha}$, and k_{HH} represent the rate constants from early G1 to late G1, from late G1 to S phase, and from S phase to G2M phase, respectively. k_{in} is described by

$$k_{in} = pRB_0 \times (k_{pRB} + k_{el}) \quad (7)$$

where pRB_0 is the baseline expression in patients.[16] The PBPK and biomarker model structures are presented in Figure 1.

2.3. PBPK and Biomarker Model Validation. The observed plasma PK parameters, such as area under the curve (AUC) and maximum concentration (C_{max}), of ABE and

https://doi.org/10.1021/acsomega.4c09472
ACS Omega 2025, 10, 9245−9256

Table 2. Geometric Mean Ccomparisons of Predicted and Observed Plasma and CSF PK Variables in Patients[a]

clinical studies	PK	dosing regimen	subject number	age range (year)	proportion of female (%)	parameters	observation	prediction	fold-error
Patnaik et al.[16]	plasma	100 mg, OD, RD	3	60 (44−73)	33	C_{min} (ng/mL)	48.7 (168%)	51 (48%)	1.05
						C_{max} (ng/mL)	102 (198%)	118 (31%)	1.16
						AUC (ng·h/mL)	1840 (172%)	3235 (67%)	1.76
		150 mg, OD, RD	3			C_{min} (ng/mL)	134 (47%)	87 (49%)	0.65
						C_{max} (ng/mL)	189 (35%)	192 (32%)	1.02
						AUC (ng·h/mL)	4305 (NR)	3413 (49%)	0.79
		100 mg, BID, RD	8			C_{min} (ng/mL)	144 (61%)	144 (47%)	1.00
						C_{max} (ng/mL)	226 (51%)	198 (37%)	0.88
						AUC (ng·h/mL)	3910 (53%)	3939 (75%)	1.01
		150 mg, BID, RD	72			C_{min} (ng/mL)	169 (95%)	174 (44%)	1.03
						C_{max} (ng/mL)	249 (86%)	250 (34%)	1.00
						AUC (ng·h/mL)	4280 (94%)	4616 (69%)	1.08
		200 mg, BID, RD	52			C_{min} (ng/mL)	197 (95%)	231 (44%)	1.17
						C_{max} (ng/mL)	298 (72%)	333 (34%)	1.12
						AUC (ng·h/mL)	5220 (70%)	6004 (69%)	1.15
Fujiwara et al.[39]		100 mg, BID, RD	3	61.3 (NR)	33	C_{min} (ng/mL)	133 (NR)	99 (33%)	0.74
						C_{max} (ng/mL)	232 (NR)	157 (18%)	0.68
						AUC (ng·h/mL)	3880 (71)	3462 (36%)	0.89
		150 mg, BID, RD	3	63.0 (NR)	33	C_{min} (ng/mL)	103 (NR)	148 (33%)	1.44
						C_{max} (ng/mL)	149 (NR)	236 (18%)	1.58
						AUC (ng·h/mL)	3960 (39%)	3768 (54%)	0.95
		200 mg, BID, RD	6	56.0 (NR)	83	C_{min} (ng/mL)	210 (89%)	198 (33%)	0.94
						C_{max} (ng/mL)	298 (64%)	315 (18%)	1.06
						AUC (ng·h/mL)	5170 (94%)	5025 (54%)	0.97
Kim et al.[40]		200 mg, BID, RD	15			C_{max} (ng/mL)	483 (41%)	396 (37%)	0.82
						AUC (ng·h/mL)	3460 (49%)	4160 (41%)	1.20
Tolaney et al.[33]		200 mg, BID, RD	58	55 (30−79)	98	C_{min} (ng/mL)	271 (73%)	309 (62%)	1.14
			27	51 (30−73)	100	C_{min} (ng/mL)	199 (61%)	294 (72%)	1.48
Patnaik et al.[16]	CSF	200 mg, BID, RD	52	60 (44−73)	33	C_{min} (ng/mL)	5.71 (61%)[b]	9.5 (89%)	1.66
Tolaney et al.[33]		200 mg, BID, RD	27	51 (30−73)	100	C_{min} (ng/mL)	16.9 (157%)[c]	13.0 (73.9%)	0.77

[a]RD: repeated doses; OD: once daily; BID: twice daily; AUC: area under PK curve; C_{max}: peak concentration; C_{min}: trough concentration at steady state. [b]ABE free concentration in CSF. [c]Total active analytes (ABE, M2, and M20) in CSF.

its three metabolites in healthy subjects following a single dose of ABE were utilized to evaluate the accuracy of predicted PK parameters (Supporting Table S1).[31] Four previously published clinical studies[16,33,39,40] were employed to assess the accuracy of predicted plasma PK parameters (AUC, C_{max}, and C_{min}) of ABE after repeated doses (Table 2). Moreover, two clinical studies[16,33] were referenced to evaluate the accuracy of predicted intracranial C_{min} of ABE and total active analytes after repeated doses (Table 2). Furthermore, a clinical study was utilized to evaluate the accuracy of predicted changes in pRB and TOPO-IIα expression over time.[16]

In the simulations, demographic characteristics of the virtual population, including dosage, subject numbers, age, and proportion of females, were derived from the respective clinical studies, as outlined in Table 2. In instances where data were unavailable, mean values from PK-Sim were employed as a surrogate for the missing information.

2.4. Sensitivity Analysis of Modeling Parameters. A sensitivity analysis was conducted to identify modeling parameters that could potentially exert a significant influence on the predicted C_{min} of the sum of ABE and its three metabolites, as well as CDK4/6 occupancy in both plasma and CSF by sum of ABE and its three metabolites. The selected parameters for analysis encompassed: f_{up}, R_{bp}, Weibull time distribution parameters, albumin level, Hct, unbound intrinsic clearance by CYP3A4 (CYP3A4 $CL_{int,u}$) and human liver microsomes (HLM $CL_{int,u}$), intrinsic transport velocity for ABCB1 and ABCG2, inhibition constant (K_i), dissociation rate constant (k_{off}), expression levels of CYP3A4, ABCB1, ABCG2, and CDK4/6_0. Additionally, a sensitivity analysis was conducted to identify modeling parameters potentially impacting the predicted expression of pRB and TOPO-IIα. The selected parameters for analysis comprised the rate constants for k_{RB}, k_{TO}, k_{HH}, and k_{el}. Alterations of ±20% were applied to each parameter during the sensitivity analysis.

https://doi.org/10.1021/acsomega.4c09472
ACS Omega 2025, 10, 9245−9256

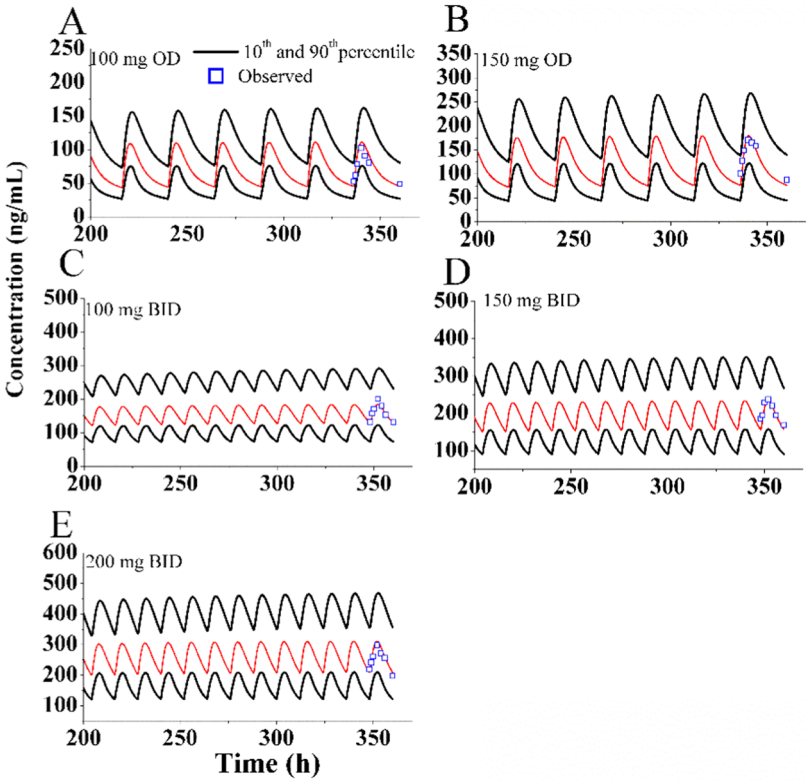

Figure 2. PBPK model-simulated and clinically observed plasma PK of ABE following repeated doses. The clinically observed plasma PKs of ABE at steady state were taken from the study by Patnaik et al. at 100 mg OD (A), 150 mg OD (B), 100 mg BID (C), 150 mg BID (D), and 200 mg BID (E).

Subsequently, the sensitivity coefficient (SC) was calculated by using the following equation:

$$SC = \Delta Y/Y \div \Delta P/P_0 \quad (8)$$

where ΔY is the alteration of predicted response; Y_0 is the initial value of response; ΔP is the alteration of model parameters; and P_0 is the initial value of parameters. The absolute value of the SC is above 1.0, suggesting that variations have a notable impact on the model predictions.

2.5. Key Factors Affecting Plasma and Intracranial C_{min} and CDK4/6 Occupancy. We investigated four specific factors for their impact on C_{min} and CDK4/6 occupancy. CPY3A4 expression levels were varied across a range of 1.2−6.0 μM, based on the studies indicating that wild-type CYP3A4 expression is approximately 2.5-fold higher than that of the CYP3A4*22 allele.[18] The brain penetrations of ABE and its active metabolites are restricted by ABCB1 and ABCG2 efflux transporters. Efflux transport for ABE and its active metabolites via ABCB1 and ABCG2 was adjusted within a range of 1- to 4-fold, as reported in previous studies.[19,20] Plasma albumin levels were set between 1.0 and 6.0 g/dL to reflect physiological values in patients.[23,24] In these simulations, the ABE dosing regimen was fixed at 200 mg. Demographic characteristics of the virtual population were aligned with those described in the clinical study by Patnaik, as detailed in Table 2.

2.6. Simulations for Optimum Dosing Regimen in BC Patients with Brain Metastasis. Based on the previous studies,[27,28] it is established that maintaining a trough CDK4/6 occupancy of at least 90% is necessary for a sufficient clinical response. Furthermore, to ensure clinical safety, it is suggested to keep the plasma C_{min} of total ABE analytes below 693 ng/mL (predicted value by the PBPK model following repeated doses of 275 mg BID). To meet these criteria in patients, various dosage regimens of ABE ranging from 100 to 400 mg OD or BID were simulated. The demographic characteristics of the virtual population were set in accordance with the clinical study conducted by Patnaik.[16] Through these simulations, the PBPK model can predict plasma C_{min} and CDK4/6 occupancy for different ABE dosage regimens, facilitating the identification of an optimal dosing strategy for clinical treatment.

3. RESULTS

3.1. PBPK Model Validation for Plasma PK. Supporting Table S1 presents the predicted and observed PK parameters for ABE and its three primary metabolites in healthy volunteers. The PBPK model accurately predicted the PK data of ABE and its metabolites within a healthy population. Figure 2 illustrates the predicted versus observed plasma concentration−time profiles for ABE after multiple oral doses in patients. These simulations effectively mirror the clinically established PK profiles. Table 2 compares the observed PK parameters of ABE with those predicted by the population-based PBPK model. The ratios of AUC, C_{max}, and C_{min} consistently fall within the acceptable range of 0.5 to 2.0, indicating a high degree of concordance between simulated and observed PK parameters.

3.2. PBPK Model Verification for Intracranial PK. As shown in Table 2, the two clinical studies[16,33] at repeated doses of 200 mg BID were used to verify the accuracy of the PBPK model prediction. The simulations showed that the predicted C_{min} in CSF is in good agreement with the observed data, with two ratios of 1.65 and 0.77. These results demonstrate that the

https://doi.org/10.1021/acsomega.4c09472
ACS Omega 2025, 10, 9245−9256

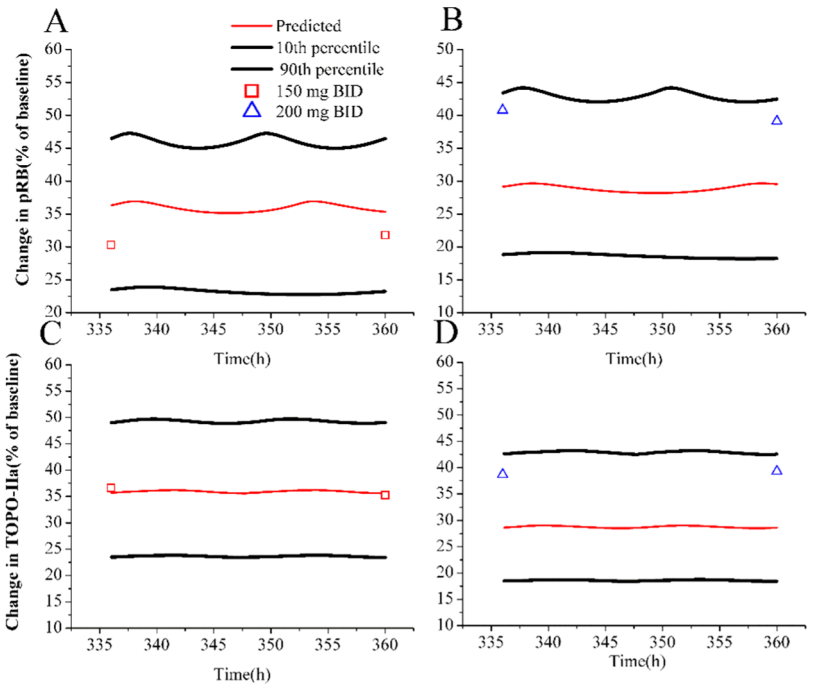

Figure 3. Simulated pharmacodynamics inhibition of pRB and TOPO-IIα expression. The simulations analyzed changes in pRB expression following doses of 150 mg of BID (A) and 200 mg of BID (B), and variations in TOPO-IIα expression receiving doses of 150 mg of BID (C) and 200 mg of BID (D) at steady state in patients. Observed data were extracted from the study conducted by Patnaik et al., capturing predose (first data point) and postdose (second data point) measurements at steady state for patients.

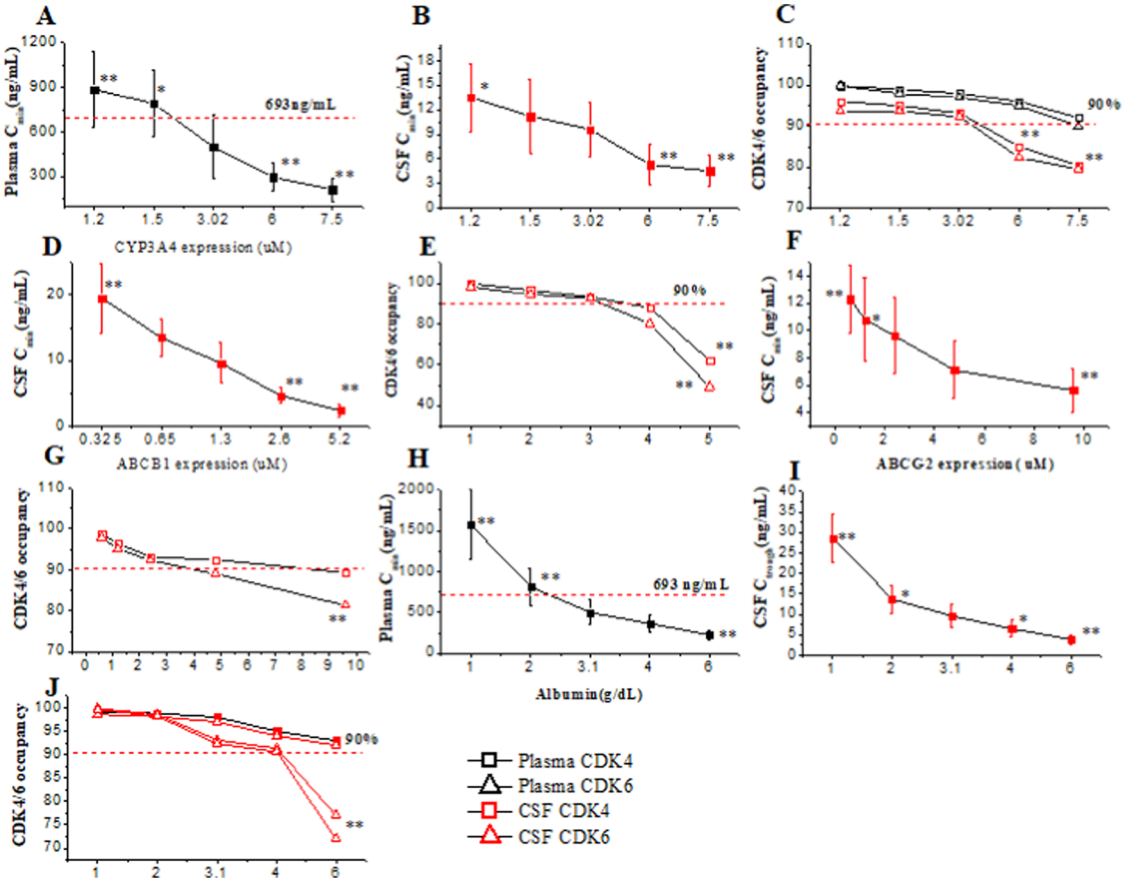

Figure 4. Factors affecting C_{min} and CDK4/6 occupancy in plasma and CSF. C_{min} in plasma and CSF, and CDK4/6 occupancy are affected by CYP3A4 expression (A–C). ABCB1 expression affects C_{min} in the CSF (D) and CDK4/6 occupancy (E). ABCG2 expression affects C_{min} in CSF (F) and CDK4/6 occupancy (G). C_{min} in plasma and CSF, and CDK4/6 occupancy is affected by albumin level expression (H–J).

https://doi.org/10.1021/acsomega.4c09472
ACS Omega 2025, 10, 9245−9256

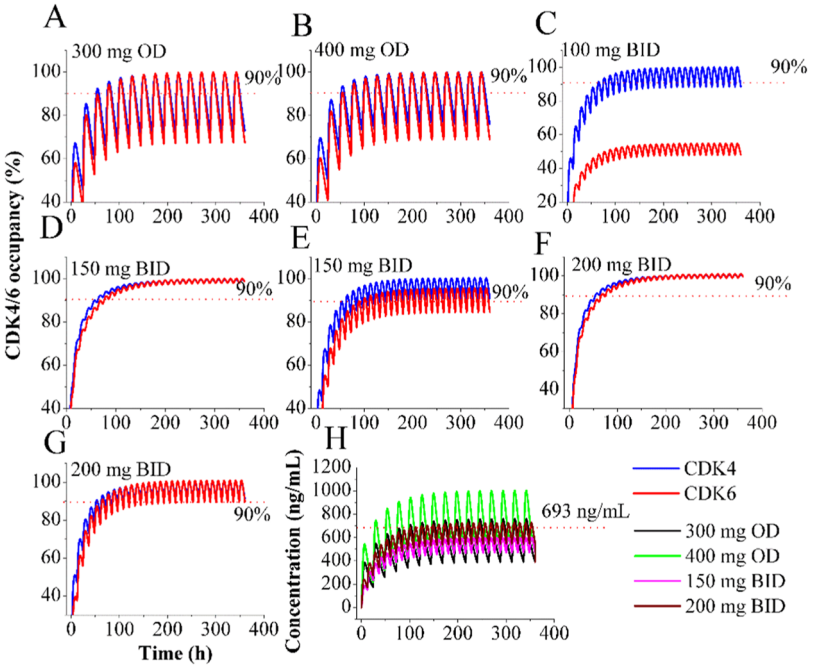

Figure 5. Simulations of the CDK4/6 occupancy by ABE. CDK4/6 occupancy was evaluated following various dosing regimens of ABE in CSF (A, B, C, E, G) and plasma (D, F). Additionally, plasma concentration−time profiles of ABE were simulated across multiple dosing regimens (H).

PBPK model has the ability to predict the intracranial PK of ABE and its three metabolites.

3.3. Biomarker Model Verification. In Figure 3, simulated changes in pRB and TOPO-IIα expression at steady state from baseline using the biomarker model are presented. The predicted changes in pRB and TOPO-IIα expression align well with the observed data at repeated doses of 150 mg BID, while they were underestimated at repeated doses of 200 mg BID. Additionally, the changes in pRB and TOPO-IIα are similar at predose and postdose, indicating sustained PD effects over the 12 h dosing interval. The simulations demonstrate that the 90% confidence interval can cover the observed pRB and TOPO-IIα expressions in patients.

3.4. Sensitivity Analysis of Modeling Parameters. The sensitivity analysis presented in Supporting Tables S2 and S3 indicates that albumin level, CYP3A4 concentration, and f_{up} were identified as sensitive parameters for C_{min} in plasma, while albumin level and f_{up} are sensitive to intracranial C_{min} among all of the selected parameters. On the other hand, the sensitivity analysis showed that no other parameters are sensitive to CDK4/6 occupancy except for ABCB1 expression, while other examined parameters are not sensitive to the change in the two biomarkers except for k_{RB}.

Although f_{up}, determined from *in vitro* experiments, was found to be a sensitive parameter,it is strongly linked to albumin levels; hence, subsequent examination of its impact on C_{min} and CDK4/6 occupancy was not performed. While ABCG2 expression did not exhibit a significant impact on C_{min} and CDK4/6 occupancy in the sensitivity analysis, however, given the association of gene polymorphisms of ABCB1 and ABCG2 with treatment outcomes in MBC patients,[41] further investigation was conducted to evaluate the effect of ABCG2 expression on C_{min} and CDK4/6 occupancy in CSF.

3.5. Factors Affecting C_{min} and CDK4/6 Occupancy in Plasma and CSF. The C_{min} of plasma total active analytes at 275 mg of BID establishes the PK threshold for clinical safety, with a defined safe C_{min} threshold of 693 ng/mL based on simulation results. Furthermore, >90% CDK4/6 occupancy is identified as the effective PD threshold. In Figure 4A−C, the impact of CYP3A4 expression on the C_{min} and CDK4/6 occupancy of total active analytes in plasma and CSF is depicted. The simulations reveal a significant effect of CYP3A4 expression on C_{min}, with a minor impact on CDK4/6 occupancy. Plasma C_{min} exceeds the established PK safety threshold when CYP3A4 expression reduces to 1.2 and 1.5 μM, while CDK4/6 occupancy in CSF falls below 90% when CYP3A4 expression is at 6.0 and 7.5 μM. Additionally, in Figure 4D,E, an increase in ABCB1 expression in patients by more than 2.0- and 4.0-fold of the original value leads to a reduction of CDK4/6 occupancy in CSF below 90%. The effect of ABCG2 expression on C_{min} in CSF and CDK4/6 occupancy by total active analytes in CSF mirrors that of ABCB1 expression (Figure 4F,G). As illustrated in Figure 4H−J, the influence of albumin levels on C_{min} and CDK4/6 occupancy in plasma and CSF is demonstrated. The simulations indicate that a reduction to 1.0 and 2.0 g/dL in plasma albumin levels can cause plasma C_{min} to exceed the PK safety threshold, while an increase to 6.0 g/dL in plasma albumin levels can lower CDK4/6 occupancy in CSF below the PD effective threshold.

3.6. Simulations in BC Patients with Brain Metastasis for Different Dosing Regimen. Intracranial CDK4/6 occupancy serves as predictors of clinical efficacy, while plasma C_{min} serves as a predictor for clinical safety. Simulations following the standard dosing regimen of ABE suggested mean plasma C_{min} is 498 ng/mL (total plasma analytes) and CDK4/6 occupancy in plasma and CSF are >90%. ABE attained sufficient CDK4/6 occupancy with the standard dosing regimen (200 mg BID), meeting the safety criterion of plasma C_{min} < 693 ng/mL and CDK4/6 occupancy >90%.

Additional simulations were conducted to refine the dosing regimens (Figure 5). Following 14 days of ABE treatment at various doses, the simulations indicated that even with a 400 mg QD dosing regimen of ABE, CDK4/6 occupancy in CSF

https://doi.org/10.1021/acsomega.4c09472
ACS Omega 2025, 10, 9245−9256

cannot exceed 90% (Figure 5B), and plasma C_{min} surpasses the PK threshold (Figure 5H). However, with 150 mg of BID of ABE, CDK4 occupancy exceeds 90% and CDK6 occupancy exceeds 80% (Figure 5E). Therefore, the simulations suggest that 150 mg and 200 mg BID are appropriate dosing regimens for brain MBC patients.

4. DISCUSSION

This study has effectively constructed a PBPK and biomarker model for ABE in brain MBC patients, facilitating simulations of C_{min} and CDK4/6 engagement in plasma and CSF, along with simulations of change in pRB and TOPO-IIα expression from baseline. To date, we have identified only four clinical plasma PK studies[16,33,39,40] and two clinical CSF PK studies,[16,33] from which original PK data can be extracted for comparison with our predicted results. Additionally, only one clinical paper has reported changes in pRB and TOPO-IIα expression in BC patients. Consequently, all relevant reported PK and PD data of ABE in patients were included in this study. The PBPK predictions were validated against four clinical plasma PK[16,33,39,40] and two clinical CSF PK studies[16,33] (Table 2 and Figure 2). The biomarker model predictions were confirmed with one clinical study[16] (Figure 3).

In this study, a plasma C_{min} of <693 ng/mL was used as predictors of clinical safety based on the exposure−response relationship for safety.[14] On the other hand, although it has been demonstrated that a >60% decrease in pRB is significantly associated with clinical efficacy,[16] the PD analyses showed a similar magnitude of inhibition of pRB and TOPO-IIα expression between the 150 mg and 200 mg BID dose levels.[14] Therefore, it is not suggested that the two biomarkers are predictive of clinical response in BC patients with ABE.[14] Given these, we used >90% CDK4/6 occupancy as predictors of clinical efficacy rather than inhibition of pRB and TOPO-IIα expression. Additionally, it is noteworthy that the biomarker model predicts changes in pRB and TOPO-IIα occurring in skin tissue, rather than in tumor tissue. Because the only alterations in pRB and TOPO-IIα within skin tissue in humans has been experimentally determined, it is assumed that the differences between the pRB and TOPO-IIα biomarker expression in tumors and skin tissue are negligible.

The current PBPK model can predict the PK and CDK4/6 occupancy of ABE and its metabolites simultaneously. It was critical to capture ABE and three active metabolites in the PBPK model due to their similar activity against CDK4/6 to ABE as well as their high concentration in plasma. ABE and its active metabolites are substrates of efflux transporters ABCB1 and ABCG2. Although these two efflux transporters have a subtle impact on plasma PK due to the high permeability and solubility of ABE, they have a significant effect on the unbound concentration of ABE and active metabolites in CSF. Therefore, $CL_{int,u}$ data for ABCB1 and ABCG2 were incorporated into the current PBPK model to more accurately predict the concentration of ABE and active metabolites in CSF. Furthermore, five modeling parameters including f_{up}, R_{bp}, CYP3A4 expression, Hct, and albumin level in patients have been modified to incorporate the current PBPK model for ensuring the predictive performance of the model in patients.

The K_p value plays a crucial role in characterizing the *in vivo* distribution of ABE and its three metabolites. According to the Rodgers and Rowland approach in PK-Sim, the simulated PK profiles did not match well with the observed data using the default K_p value. Therefore, the K_p scale was optimized to 5.0 for a better fit with the observed PK profiles. In some simulations conducted for humans, kinase concentration values ranging from 0.01 to 0.1 μM are universally used.[41−44] Considering that protein kinases are often overexpressed in patients,[28,45] for diseased humans, the initial levels of kinase targets are set at a higher constant value of 0.1 μM in this study. Furthermore, sensitivity analysis of modeling parameters on CDK4/6 occupancy revealed that CDK4/6 expressions are not sensitive to CDK4/6 occupancy (Supporting Table S3). Therefore, a value of 0.1 μM for CDK4/6 expression should be acceptable.

The sensitivity analysis plays a crucial role in the PBPK model. This analysis enables us to understand the degree of dependence of C_{min} and CDK4/6 occupancy on various modeling parameters, thus identifying key factors in complex situations, optimizing the model development process, and improving prediction accuracy. In this study, the sensitivity analysis indicates that the albumin level, CYP3A4 concentration, f_{up}, and ABCB1 expression were sensitive parameters. In our further study, we have also demonstrated that the albumin level, CYP3A4 concentration, and ABCB1 expression can influence the efficacy and safety of ABE in clinical treatment (Figure 4). Additionally, strong associations between albumin level, ABCB1 and ABCG2 expression have been observed in relation to clinical treatment outcomes.[25,46] Our sensitivity analysis has revealed that f_{up}, CYP3A4 expression, and albumin levels substantially affect the PK and CDK4/6 occupancy of ABE and its metabolites. Consequently, it is better to calibrate these parameters within the PBPK model to better fit the MBC population, thereby facilitating more accurate predictions.

Furthermore, the PBPK model identified four key factors with significant impacts on C_{min} and CDK4/6 in plasma and CSF (Figure 4). The variation in CYP3A4 expression can significantly affect PK and occupancy of ABE, and this can be explained by 89% of ABE metabolism being attributed to CYP3A4.[31] In a previous study,[41] carriers of the CYP3A422 allele have a high risk of adverse events. Our simulations showed that plasma C_{min} exceeds the safe threshold in BC patients when CYP3A4 expression was set at 1.2 μM (Figure 4A, expression level corresponds to carriers of the CYP3A422 allele). The simulations also demonstrated that ABCB1 and ABCG2 expression is strongly linked to clinical CSF exposure and efficacy of ABE (Figure 4D−G). These results are in good agreement with the observed data in the paper,[46] where gene polymorphisms of ABCB1 and ABCG2 exhibited significant associations with clinical treatment outcomes in MBC patients. Albumin varies widely in patients, as multiple papers[21,25] have shown that plasma albumin level is strongly associated with clinical efficacy and safety. In these simulations, it has been demonstrated that C_{min} and CDK4/6 occupancy were significantly affected by albumin level (Figure 4H−J). This result is also consistent with the clinically observed result,[25] where among patients with albumin levels >4.0 g/dl, the incidence of ABE-induced serious adverse events was significantly lower due to relatively lower plasma C_{min}.

Various dosing strategies for ABE in MBC treatment were simulated to assess their CDK4/6 occupancy and potential clinical toxicities (Figure 5). In contrast, ABE exhibited a favorable safety profile and achieved sustained CDK4/6 occupancy in CSF at doses of 150 and 200 mg of BID. However, even a single dose of 400 mg cannot achieve sufficient CDK4/6 occupancy in the CSF. Therefore, dosing

https://doi.org/10.1021/acsomega.4c09472
ACS Omega 2025, 10, 9245−9256

regimens of 150 and 200 mg of BID were recommended as suitable for brain MBC treatment. These simulations align well with clinically observed pharmacodynamic effects.[16]

In clinical practice, the plasma albumin level and polymorphisms of CYP3A4 of patients can be determined and analyzed by collecting blood samples. Additionally, to assess ABCB1 and ABCG2 expression, tissue samples, such as skin biopsies or the isolation of peripheral blood mononuclear cells from blood samples, can be employed. These measured values can then be integrated into our PBPK model to evaluate the potential efficacy and safety outcomes for patients with brain MBC.

There are some assumptions in the current PBPK model. It is assumed that the transport of ABE across the capillary membrane is governed by the permeability limits. To simulate the free concentration of ABE within the CSF, the unbound concentration in the interstitial fluid is equivalent to the free concentration within the CSF. Moreover, due to the unavailability of experimental data, the k_{off} values for three metabolites were considered uniform with ABE. Additionally, the changes in the expression of pRB and TOPO-IIα, which were experimentally determined, were derived from skin tissue sources. It was assumed that the discrepancies in the expression changes of pRB and TOPO-IIα between the tumor and skin tissues were minimal. Additionally, the model currently has several limitations. Its first limitation is the absence of experimentally confirmed CDK4/6 occupancy data to verify the predictive accuracy of the PBPK model. Additionally, only one clinical study was obtained to validate the biomarker model. Furthermore, with the exception of the six parameters previously mentioned, the remaining model parameters were assumed to remain consistent with normal physiological conditions for ABE. Another challenge for the PBPK model is the lack of assessment regarding the impact of CDK4/6 cellular half-life on CDK4/6 occupancy However, kinase synthetic half-life in cells have been demonstrated to play an important role in target occupancy.[28] Finally, of the four key factors identified by the PBPK model, however, the impact of CYP3A4 expression lacks clinical experimental validation. Given that ABE and its three metabolites are highly lipophilic, as indicated their log P values, they were assigned the same K_p scale value. However, this value may not entirely represent their actual *in vivo* distribution.

5. CONCLUSIONS

In conclusion, this study successfully developed and validated a PBPK model for ABE in brain MBC patients. The innovation of the current research is reflected in the following three aspects: (i) the current study is the first to define the clinical efficacy and safe threshold for ABE; (ii) the model is first proposed to simulate the CDK4/6 occupancy in both plasma and CSF for ABE and its three active metabolites; (iii) furthermore, the research uniquely identifies four key factors that significantly impact the C_{min} and CDK4/6 occupancy. The PBPK model offers valuable guidance for optimizing ABE dosing regimens in patient populations.

■ ASSOCIATED CONTENT

Data Availability Statement

The study contains original contributions that are detailed in the article and Supporting Information. For any further inquiries, please feel free to reach out to the corresponding authors. All data generated are included in this published article and Supporting Material that is available online.

Supporting Information

The Supporting Information is available free of charge at https://pubs.acs.org/doi/10.1021/acsomega.4c09472.

Geometric mean comparisons of predicted and observed plasma PK variables in healthy subjects (Table S1); sensitivity analysis of modeling parameters on C_{min} (Table S2), and sensitivity analysis of modeling parameters on CDK4/6 occupancy and two biomarkers (Table S3) (PDF)

■ AUTHOR INFORMATION

Corresponding Author

Ren Lang − *Beijing Chaoyang Hospital, Beijing 100020, China*; Email: Wzfb2021@163.com

Authors

Chao Zhang − *Beijing Chaoyang Hospital, Beijing 100020, China*; orcid.org/0009-0006-0028-4017

Shan Li − *Beijing Chaoyang Hospital, Beijing 100020, China*

Jiawei Ren − *North China Electric Power University, Beijing 102206, China*; orcid.org/0000-0002-5701-4919

Complete contact information is available at: https://pubs.acs.org/10.1021/acsomega.4c09472

Author Contributions

C.Z. authored the manuscript text and created all tables and figures, while S.L. was accountable for data curation. J.W.R. was accountable for software calculation; R.L. made contributions to investigation, methodology conceptualization, formal analysis, and supervision. The manuscript was reviewed by all authors.

Funding

The research in this publication does not receive any funding support.

Notes

The authors declare no competing financial interest.

■ ACKNOWLEDGMENTS

Thank you to all of the authors for their assistance and cooperation.

■ REFERENCES

(1) Trentham-Dietz, A.; Chapman, C. H.; Bird, J.; Gangnon, R. E. Recent changes in the patterns of breast cancer as a proportion of all deaths according to race and ethnicity. *Epidemiology* **2021**, *32* (6), 904−913.

(2) Tripathy, D.; Brufsky, A.; Cobleigh, M.; Jahanzeb, M.; Kaufman, P. A.; Mason, G.; Hurvitz, S. A.; et al. De novo versus recurrent HER2-positive metastatic breast cancer: patient characteristics, treatment, and survival from the SystHERs registry. *Oncologist* **2020**, *25* (2), e214−e222.

(3) Cserni, G.; Quinn, C. M.; Foschini, M. P.; Bianchi, S.; Callagy, G.; Chmielik, E.; European. Working Group for Breast Screening Pathology; et al. Triple-negative breast cancer histological subtypes with a favourable prognosis. *Cancers* **2021**, *13* (22), No. 5694.

(4) Li, H.; Wang, P.; Liu, J.; Liu, W.; Wu, X.; Ding, J.; Pan, G.; et al. Hypermethylation of lncRNA MEG3 impairs chemosensitivity of breast cancer cells. *J. Clin. Lab. Anal.* **2020**, *34* (9), No. e23369.

(5) Witzel, I.; Oliveira-Ferrer, L.; Pantel, K.; Müller, V.; Wikman, H. Breast cancer brain metastases: biology and new clinical perspectives. *Breast Cancer Res.* **2016**, *18*, No. 8.

(6) Kuksis, M.; Gao, Y.; Tran, W.; Hoey, C.; Kiss, A.; Komorowski, A. S.; Jerzak, K. J.; et al. The incidence of brain metastases among patients with metastatic breast cancer: a systematic review and meta-analysis. *Neuro-Oncology* **2021**, *23* (6), 894−904.
(7) Arvanitis, C. D.; Ferraro, G. B.; Jain, R. K. The blood−brain barrier and blood−tumour barrier in brain tumours and metastases. *Nat. Rev. Cancer* **2020**, *20* (1), 26−41.
(8) Saleban, M.; Harris, E. L.; Poulter, J. A. D-type Cyclins in Development and Disease. *Genes* **2023**, *14* (7), No. 1445.
(9) Fassl, A.; Geng, Y.; Sicinski, P. CDK4 and CDK6 kinases: From basic science to cancer therapy. *Science* **2022**, *375* (6577), No. eabc1495.
(10) Goel, S.; Bergholz, J. S.; Zhao, J. J. Targeting CDK4 and CDK6 in cancer. *Nat. Rev. Cancer* **2022**, *22* (6), 356−372.
(11) Alexandrou, S.; George, S. M.; Ormandy, C. J.; Lim, E.; Oakes, S. R.; Caldon, C. E. The proliferative and apoptotic landscape of basal-like breast cancer. *Int. J. Mol. Sci.* **2019**, *20* (3), No. 667.
(12) Wang, X.; Zhao, S.; Xin, Q.; Zhang, Y.; Wang, K.; Li, M. Recent progress of CDK4/6 inhibitors' current practice in breast cancer. *Cancer Gene Ther.* **2024**, *31*, 1283−1291.
(13) Groenland, S. L.; Martínez-Chávez, A.; van Dongen, M. G.; Beijnen, J. H.; Schinkel, A. H.; Huitema, A. D.; Steeghs, N. Clinical pharmacokinetics and pharmacodynamics of the cyclin-dependent kinase 4 and 6 inhibitors palbociclib, ribociclib, and abemaciclib. *Clin. Pharmacokinet.* **2020**, *59* (12), 1501−1520.
(14) Food and Drug Administration (FDA) Center for Drug Evaluation and Research. https://www.accessdata.fda.gov/drugsatfda_docs/nda/2018/208855Orig1s000MultidisciplineR.pdf.
(15) Martínez-Chávez, A.; Loos, N. H.; Lebre, M. C.; Tibben, M. M.; Rosing, H.; Beijnen, J. H.; Schinkel, A. H. ABCB1 and ABCG2 limit brain penetration and, together with CYP3A4, total plasma exposure of abemaciclib and its active metabolites. *Pharmacol. Res.* **2022**, *178*, No. 105954.
(16) Patnaik, A.; Rosen, L. S.; Tolaney, S. M.; Tolcher, A. W.; Goldman, J. W.; Gandhi, L.; Shapiro, G. I.; et al. Efficacy and safety of abemaciclib, an inhibitor of CDK4 and CDK6, for patients with breast cancer, non−small cell lung cancer, and other solid tumors. *Cancer Discovery* **2016**, *6* (7), 740−753.
(17) Kubeczko, M.; Jarząb, M.; Krzywon, A.; Gräupner, D.; Polakiewicz-Gilowska, A.; Gabryś, D. Efficacy of CDK 4/6 inhibitors and radiotherapy in breast cancer patients with brain metastases. *J. Clin. Med.* **2023**, *12* (5), No. 2044.
(18) Alqahtani, S.; Kaddoumi, A. Development of a physiologically based pharmacokinetic/pharmacodynamic model to predict the impact of genetic polymorphisms on the pharmacokinetics and pharmacodynamics represented by receptor/transporter occupancy of central nervous system drugs. *Clin. Pharmacokinet.* **2016**, *55*, 957−969.
(19) Li, J.; Cusatis, G.; Brahmer, J.; Sparreboom, A.; Robey, R. W.; Bates, S. E.; Hidalgo, M.; Baker, S. Association of variant ABCG2 and the pharmacokinetics of epidermal growth factor receptor tyrosine kinase inhibitors in cancer patients. *Cancer Biol. Ther.* **2007**, *6* (3), 432−438.
(20) Salama, N. N.; Yang, Z.; Bui, T.; Ho, R. J. MDR1 haplotypes significantly minimize intracellular uptake and transcellular P-gp substrate transport in recombinant LLC-PK1 cells. *J. Pharm. Sci.* **2006**, *95* (10), 2293−2308.
(21) Hashino, Y.; Hatsuyama, T.; Iwayama, K.; Hoshi, T.; Wakamoto, A.; Ohtaki, K.; Sato, H. The relationship between efficacy and safety of osimertinib blood concentration in patients with EGFR mutation-positive lung cancer: a prospective observational study. *In Vivo* **2023**, *37* (6), 2669−2677.
(22) Liang, F.; Zhang, Y.; Xue, Q.; Yao, N. Exploring inter-ethnic and inter-patient variability and optimal dosing of osimertinib: a physiologically based pharmacokinetic modeling approach. *Front. Pharmacol.* **2024**, *15*, No. 1363259.
(23) Lis, C. G.; Grutsch, J. F.; Vashi, P. G.; Lammersfeld, C. A. Is serum albumin an independent predictor of survival in patients with breast cancer? *J. Parenter. Enteral Nutr.* **2003**, *27* (1), 10−15.
(24) Food and Drug Administration (FDA) Center for Drug Evaluation and Research. https://www.accessdata.fda.gov/drugsatfda_docs/nda/2015/208065Orig1s000ClinPharmR.pdf.
(25) Nakatsukasa, H.; Takahashi, M.; Takahashi, K.; Takashima, T.; Asano, Y.; Morisaki, T.; Nakamura, Y.; et al. The Cyclin-Dependent Kinase 4/6 Inhibitor Abemaciclib Is Tolerated Better than Palbociclib by Advanced Breast Cancer Patients with High Serum Albumin Levels. *Biol. Pharm. Bull.* **2022**, *45* (10), 1476−1481.
(26) Adiwidjaja, J.; Gross, A. S.; Boddy, A. V.; McLachlan, A. J. Physiologically-based pharmacokinetic model predictions of inter-ethnic differences in imatinib pharmacokinetics and dosing regimens. *Br. J. Clin. Pharmacol.* **2022**, *88* (4), 1735−1750.
(27) Tam, C. S.; Ou, Y. C.; Trotman, J.; Opat, S. Clinical pharmacology and PK/PD translation of the second-generation Bruton's tyrosine kinase inhibitor, zanubrutinib. *Expert Rev. Clin. Pharmacol.* **2021**, *14* (11), 1329−1344.
(28) Xu, L.; Yu, S.; Liu, H.; Yi, B.; Wang, G.; Liu, Y. Physiologically based pharmacokinetic combined BTK occupancy modeling for optimal dosing regimen prediction of acalabrutinib in patients alone, with different CYP3A4 variants, co-administered with CYP3A4 modulators and with hepatic impairment. *Eur. J. Clin. Pharmacol.* **2022**, *78* (9), 1435−1446.
(29) Gaohua, L.; Neuhoff, S.; Johnson, T. N.; Rostami-Hodjegan, A.; Jamei, M. Development of a permeability-limited model of the human brain and cerebrospinal fluid (CSF) to integrate known physiological and biological knowledge: Estimating time varying CSF drug concentrations and their variability using in vitro data. *Drug Metab. Pharmacokinet.* **2016**, *31* (3), 224−233.
(30) Alsmadi, M. T. M.; AL-Daoud, N. M.; Jaradat, M. M.; Alzughoul, S. B.; Abu Kwiak, A. D.; Abu Laila, S. S.; Abu Kassab, H. T.; et al. Physiologically-based pharmacokinetic model for alectinib, ruxolitinib, and panobinostat in the presence of cancer, renal impairment, and hepatic impairment. *Biopharm. Drug Dispos.* **2021**, *42* (6), 263−284.
(31) Posada, M. M.; Morse, B. L.; Turner, P. K.; Kulanthaivel, P.; Hall, S. D.; Dickinson, G. L. Predicting clinical effects of CYP3A4 modulators on abemaciclib and active metabolites exposure using physiologically based pharmacokinetic modeling. *J. Clin. Pharmacol.* **2020**, *60* (7), 915−930.
(32) Li, J.; Jiang, J.; Wu, J.; Bao, X.; Sanai, N. Physiologically based pharmacokinetic modeling of central nervous system pharmacokinetics of CDK4/6 inhibitors to guide selection of drug and dosing regimen for brain cancer treatment. *Clin. Pharmacol. Ther.* **2021**, *109* (2), 494−506.
(33) Tolaney, S. M.; Sahebjam, S.; Le Rhun, E.; Bachelot, T.; Kabos, P.; Awada, A.; Anders, C. K.; et al. A phase II study of abemaciclib in patients with brain metastases secondary to hormone receptor−positive breast cancer. *Clin. Cancer Res.* **2020**, *26* (20), 5310−5319.
(34) Bao, X.; Wu, J.; Xie, Y.; Kim, S.; Michelhaugh, S.; Jiang, J.; Li, J.; et al. Protein expression and functional relevance of efflux and uptake drug transporters at the blood−brain barrier of human brain and glioblastoma. *Clin. Pharmacol. Ther.* **2020**, *107* (5), 1116−1127.
(35) Torres-Guzmán, R.; Calsina, B.; Hermoso, A.; Baquero, C.; Alvarez, B.; Amat, J.; Lallena, M. J.; et al. Preclinical characterization of abemaciclib in hormone receptor positive breast cancer. *Oncotarget* **2017**, *8* (41), No. 69493.
(36) Inoue, T.; Emi, A.; Vasta, J. D.; Robers, M. B.; Kawase, Y. Abstract C085: A new method to determine drug-target residence time of kinase inhibitors in living cells. *Mol. Cancer Ther.* **2019**, *18*, No. C085.
(37) Tate, S. C.; Cai, S.; Ajamie, R. T.; Burke, T.; Beckmann, R. P.; Chan, E. M.; Cronier, D. M.; et al. Semi-mechanistic pharmacokinetic/pharmacodynamic modeling of the antitumor activity of LY2835219, a new cyclin-dependent kinase 4/6 inhibitor, in mice bearing human tumor xenografts. *Clin. Cancer Res.* **2014**, *20* (14), 3763−3774.
(38) Wong, Y. C.; Centanni, M.; de Lange, E. C. Physiologically based modeling approach to predict dopamine D2 receptor

https://doi.org/10.1021/acsomega.4c09472
ACS Omega 2025, 10, 9245−9256

occupancy of antipsychotics in brain: translation from rat to human. *J. Clin. Pharmacol.* **2019**, *59* (5), 731−747.
(39) Fujiwara, Y.; Tamura, K.; Kondo, S.; Tanabe, Y.; Iwasa, S.; Shimomura, A.; Yamamoto, N.; et al. Phase 1 study of abemaciclib, an inhibitor of CDK 4 and 6, as a single agent for Japanese patients with advanced cancer. *Cancer Chemother. Pharmacol.* **2016**, *78*, 281−288.
(40) Kim, E. S.; Kelly, K.; Paz-Ares, L. G.; Garrido, P.; Jalal, S.; Mahadevan, D.; Goldman, J. W.; et al. Abemaciclib in combination with single-agent options in patients with stage IV non−small cell lung cancer: a phase Ib study. *Clin. Cancer Res.* **2018**, *24* (22), 5543−5551.
(41) Georgi, V.; Schiele, F.; Berger, B. T.; Steffen, A.; Zapata, P. A. M.; Briem, H.; Fernández-Montalván, A.; et al. Binding kinetics survey of the drugged kinome. *J. Am. Chem. Soc.* **2018**, *140* (46), 15774−15782.
(42) Landersdorfer, C. B.; He, Y. L.; Jusko, W. J Mechanism-based population pharmacokinetic modelling in diabetes: vildagliptin as a tight binding inhibitor and substrate of dipeptidyl peptidase IV. *Br. J. Clin. Pharmacol.* **2012**, *73* (3), 391−401.
(43) de Witte, W. E.; Wong, Y. C.; Nederpelt, I.; Heitman, L. H.; Danhof, M.; van der Graaf, P. H.; Gilissen, R. A.; de Lange, E. C. Mechanistic models enable the rational use of in vitro drug-target binding kinetics for better drug effects in patients. *Expert Opin. Drug Discovery* **2016**, *11* (1), 45−63.
(44) de Witte, W. E.; Danhof, M.; van der Graaf, P. H.; de Lange, E. C. In vivo target residence time and kinetic selectivity: the association rate constant as determinant. *Trends Pharmacol. Sci.* **2016**, *37* (10), 831−842.
(45) Shaw, A. T.; Felip, E.; Bauer, T. M.; Besse, B.; Navarro, A.; Postel-Vinay, S.; Solomon, B. J.; et al. Lorlatinib in non-small-cell lung cancer with ALK or ROS1 rearrangement: an international, multicentre, open-label, single-arm first-in-man phase 1 trial. *Lancet Oncol.* **2017**, *18* (12), 1590−1599.
(46) Peruzzi, E.; Gerratana, L.; Montico, M.; Posocco, B.; Corsetti, S.; Bartoletti, M.; Roncato, R.; et al. Association of ADME gene polymorphisms on toxicity to CDK4/6 inhibitors in patients with HR + HER2-metastatic breast cancer. *Biomed. Pharmacother.* **2023**, *167*, No. 115479.

https://doi.org/10.1021/acsomega.4c09472
ACS Omega 2025, 10, 9245−9256